IEEE Access
Multidisciplinary | Rapid Review | Open Access Journal

Received July 29, 2020, accepted August 5, 2020, date of publication August 10, 2020, date of current version August 31, 2020.

Digital Object Identifier 10.1109/ACCESS.2020.3015278

Structure Electromagnetic Force Analysis of WPT System Under Fault Conditions

XIAN ZHANG, FENGXIAN WANG, XUEJING NI, YANAN REN, AND QINGXIN YANG
Tianjin Key Laboratory of Advanced Electrical Engineering and Energy Technology, Tianjin Polytechnic University, Tianjin 300387, China
Corresponding author: Fengxian Wang (wfx_tjpu@yeah.net)

This work was supported by the National Natural Science Foundation of China under Grant 51677132 and Grant 51977147.

ABSTRACT In the high-frequency electromagnetic field, the coupling of the wireless power transfer (WPT) system is affected by the electromagnetic force (EMF). The fault conditions will strengthen the influence, cause the damage of magnetic shielding structure, coil deformation, insulation damage and so on. In order to ensure the safe and stable operation of the WPT system, it is necessary to study the local EMF distribution of the coupling mechanism under the fault condition of WPT system. In this paper, the series to series (SS) compensation structure is taken as an example to analyze the changes of electrical parameters of WPT system under typical faults, and determines that the open load fault has the greatest impact on the system. The WPT system with groove-shaped magnetic shield structure is selected as the research object. Establish a mathematical model for calculating the EMF of the WPT system combining the field-path coupling time-step finite element method and the Maxwell stress method, the distribution law of local EMF of magnetic shielding structure when the load is open is analyzed and calculated. At the same time, an experimental platform is built to verify the effectiveness of the method. According to the distribution characteristics of EMF, the smoothing scheme based on variable-turn-pitch planar coil is proposed. The new coil structure obtained by the SNOPT algorithm, compared with the equi-turn-pitch planar coil, the overall force on the coupling mechanism of transmitting end under the open circuit fault at the receiving end is reduced by 86.24%. This study provides a theoretical reference for the optimal design of coupling mechanism of WPT system.

INDEX TERMS Wireless power transfer, failure analysis, electromagnetic force, stress distribution, smoothing scheme.

I. INTRODUCTION

Wireless power transmission (WPT) technology overcomes the shortcomings and limitations of contact power transmission, and draws wide attention of the commercial electric vehicle industry [1], rail transportation industry [2], port container transportation industry and other fields [3]–[5]. WPT technology realizes the WPT through the coupling of high-frequency electromagnetic field between coupling mechanisms. The high-frequency electromagnetic field will produce electromagnetic force (EMF) on the coupling mechanism and metal foreign matters in the system [6]. The failure of the WPT system will increase the impact of EMF, leading to the damage and fatigue of coupling mechanism components, and affecting the safe operation of the system.

The associate editor coordinating the review of this manuscript and approving it for publication was Zhilei Yao.

Theoretical analysis and calculation methods of EMF have been developed at home and abroad. In reference [7], the distribution of EMF on the coil of dry-type transformer under short-circuit fault is studied. In reference [8], the characteristics of EMF considering different types of resonant current are derived, and the multi physical field model of PMSM is established. In reference [9], the phenomenon of transformer vibration caused by EMF is rated by the method of sound pressure. In reference [10], the influence of the material characteristics and geometric structure of the iron core on the stress of the winding of the intermediate frequency transformer is analyzed. In reference [11], an improved superposition method is proposed to measure the unbalanced EMF of PMSM under eccentric rotation. At present, the analysis and calculation of EMF are mainly focused on common electrical equipment. The research on WPT system is mainly focused on impedance matching [12], coil structure optimization [13], transmission distance [14], etc. The research on EMF of WPT

system is still in its infancy [15]–[18]. In reference [17], a design scheme of micro robot for WPT is proposed, which can supply wireless power and provide propulsion force for micro robot by using electromagnetic moment. In reference [18], a launch coil structure composed of three pairs of Helmholtz coils is designed to realize omnidirectional rotation of micro robot. In reference [15], [16], the problem of EMF on WPT system is studied, and preliminary and clear conclusions are obtained. The coupling coil and shielding material are mainly affected by the EMF in the vertical direction, and the steady-state EMF on them is in the opposite direction and repels each other. The long-term vibration will cause structural fatigue of the coupling mechanism of the WPT system, and fault conditions will exacerbate this effect. However, there is no literature analysis on the local EMF of the coupling mechanism when the WPT system breaks down suddenly.

In this paper, the local EMF distribution of the coupling mechanism under the fault condition of the WPT system is taken as the research object. It analyzes and compares the impact of various typical faults on the WPT system, and determines that the open circuit fault at the receiver has the greatest impact on the WPT system. The numerical analysis and calculation of electromagnetic field are carried out, and the mathematical model of EMF calculation of WPT system is established by combining the field-circuit coupling time-step finite element method and Maxwell stress method. The magnetic shielding structure of the WPT system is usually a multi strand groove structure, which provides wire inlay support and magnetic flux channel to enhance the coupling effect. Through the finite element software to build the simulation model of the multi strand groove structure, the local EMF of the coupling mechanism and the distribution and change rule of the local EMF in the key area of the groove wall are obtained. Finally, an experimental platform is built to verify the correctness of the theoretical model. In this paper, the EMF distribution and change rule of coupling mechanism in case of sudden failure of WPT system are studied, which can provide guiding role in the structural optimization design of coupling mechanism.

II. FAILURE MODE OF WPT SYSTEM

A. FAILURE ANALYSIS OF WPT SYSTEM

Typical faults of WPT system include: ground and disconnection of bus at transmitting end, damage of inverter bridge at transmitting end, open circuit of bus ground and load at receiving end, damage of rectifier bridge at receiving end [19]. By summarizing the fault characteristics, the fault of WPT system can be regarded as any periodic combination of open circuit and short circuit at transmitting end and open circuit and short circuit at receiving end. In this paper, the series to series (SS) compensation structure is taken as an example to analyze the changes of electrical parameters of WPT system based on the SS type under typical faults.

When an open circuit fault occurs, the system can be regarded as a second-order underdamped system because the unilateral circuit is in case of open circuit. Figure 1 is the topological structure of the system in case of open circuit fault, in which t_1 and t_2 respectively correspond to the open circuit fault of the transmitting end and the open circuit fault of the receiving end.

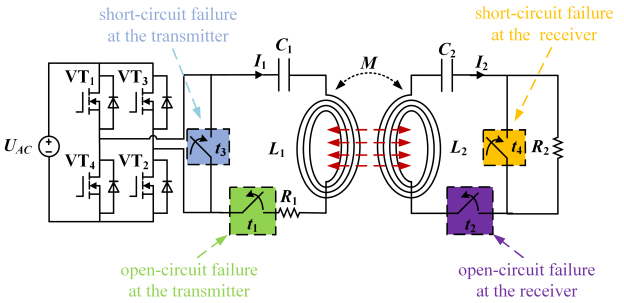

FIGURE 1. Topology diagram of WPT system based on the SS type under fault.

Assuming that the output of inverter bridge is an ideal sine wave with amplitude U_m, the attenuation coefficient of resonant circuit on the transmitting side is defined as α_1, the attenuation coefficient of resonant circuit on the receiving side as α_2, and the resonant frequency as ω, where $\alpha_i = R_i/2L_i, (i = 1, 2)$. When the system has an open circuit fault, the coil current value at the fault end is zero, and the compensation capacitance voltage value at the non fault end is respectively (1) and (2), as shown at the bottom of the page.

In the formula, L_1, R_1 and C_1 are the inductance, resistance and compensation capacitance of the transmitting coil; L_2, R_2 and C_2 are the inductance, resistance and compensation capacitance of the receiving coil; $u_{c1}(0_+)$, $i_{c1}(0_+)$ are the voltage value of the compensation capacitance at the transmitting end and the current value of the coil at the transmitting end in case of fault; $u_{c2}(0_+)$, $i_{l2}(0_+)$ are the voltage value of the compensation capacitance at the receiving end and the current

$$u_{c1}(t) = e^{-\alpha_1 t}\left(u_{c1}(0_+)\cos\left(\sqrt{\omega^2-\alpha_1^2}t\right) + \frac{i_{l1}(0_+)+\alpha C_1 u_{c1}(0_+)}{C_1\sqrt{\omega^2-\alpha_1^2}}\sin\left(\sqrt{\omega^2-\alpha_1^2}t\right)\right) + U_m\frac{\sqrt{L_1C_1}}{R_1C_1}\sin(\varphi-\omega t) \quad (1)$$

$$u_{c2}(t) = e^{-\alpha_2 t}\left(u_{c2}(0_+)\cos\left(\sqrt{\omega^2-\alpha_2^2}t\right) + \frac{i_{l2}(0_+)+\alpha C_2 u_{c2}(0_+)}{C_2\sqrt{\omega^2-\alpha_2^2}}\sin\left(\sqrt{\omega^2-\alpha_2^2}t\right)\right) \quad (2)$$

value of the coil at the receiving end respectively in case of fault. $u_{c1}(t)$ and $u_{c2}(t)$ are the voltage values of compensation capacitance at the transmitting end and receiving end respectively.

When the short-circuit fault occurs, the system can be regarded as a fourth-order damped system because the two-sided circuits are in the cascade state, and the receiving end has the source term when the short-circuit fault occurs. Figure 1 shows the topological structure diagram of system in the case of short circuit fault, in which t_3 and t_4 respectively correspond to the short circuit fault at the transmitting end and the short circuit fault at the receiving end. After the short-circuit fault at the transmitting end, the system can be regarded as a closed fourth-order system. Under the damping effect, the oscillation attenuation of the coil current at the transmitting end and the coil current at the receiving end is zero. In the dynamic process, the current value is lower than the stable operation value. In the case of short circuit fault at receiving end, the coil current of receiving end containing source term will oscillate and detuning, and it will be stable finally under the damping effect. Under stable state, the current value of the receiving end coil is:

$$i_2 = -\frac{1}{M}\int_{t_0}^{t} u_s(\xi)\, d\zeta \tag{3}$$

In the formula, M is the mutual inductance between the transmitting coil and the receiving coil, and $u_s(\zeta)$ is the output voltage value of the inverter bridge. Assume that the system electrification parameters are as shown in Table. 1.

TABLE 1. Electrical energy parameters of the WPT system.

Parameter name	Setting value	Description
L	36 μH	Coil inductance
M	7.5 μH	Coil mutual inductance
C	7 μF	Resonant capacitor
R_1	0.1 Ω	Primary resistance

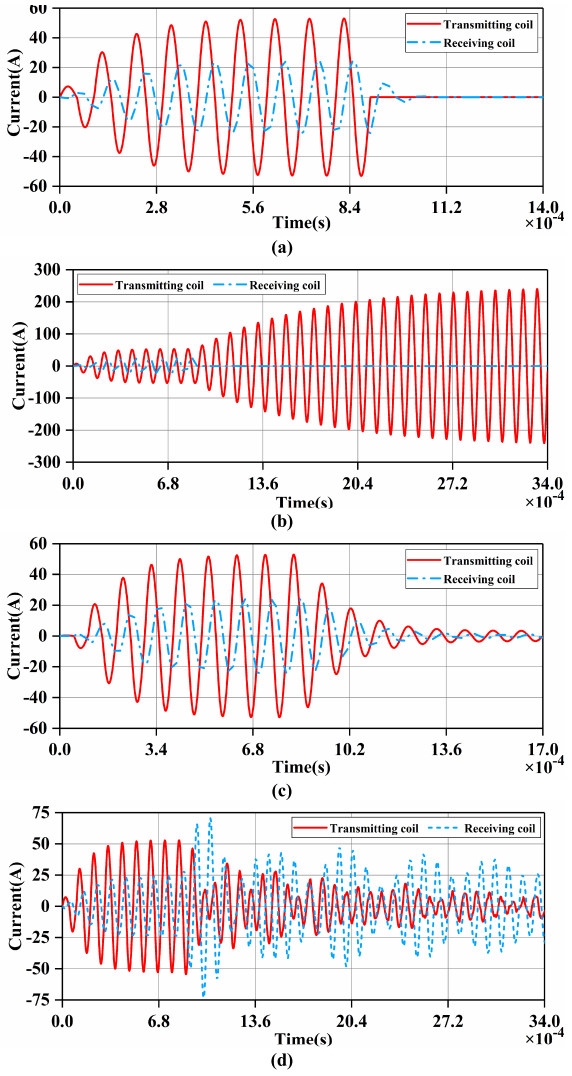

FIGURE 2. Typical failure of the WPT based on the SS type system: (a) Open circuit fault at transmitting end, (b) Open circuit fault at receiving end, (c) Short circuit fault at transmitting end, (d) Short circuit fault at receiving end.

In this case, the waveforms of the coil current at the transmitting end and the coil current at the receiving end are as shown in Figure 2. As shown in Figure 2(a), the transmitting end is a second-order underdamped oscillation circuit. After the fault occurs, the coil current at the transmitting end is zero, and at the same time, the coil current at the receiving end is reduced to zero after two oscillation periods; when the receiving end is under open circuit fault, as shown in Figure 2(b), it is a second-order underdamped oscillation circuit. After the fault occurs, the coil current at the receiving end will be zero instantly, and the coil current at the transmitting end will reach the maximum amplitude after 20 oscillation periods, which is about 4 times of the current amplitude under steady-state operation; when the short-circuit fault at the transmitting end is as shown in Figure 2(c), it is a fourth-order damped oscillation circuit. After the fault occurs, the coil current oscillation of the transmitting end and the receiving end attenuates and reaches a stable state after three oscillation periods; when the receiving end is under short circuit fault, as shown in Figure 2(d), it is a fourth-order damped oscillation circuit with source term. After the fault occurs, the system appears the phenomenon of detuning, after seven periods of detuning, it reaches a stable state, and the dynamic process will produce the phenomenon of overshoot which is about three times of the current amplitude under the steady-state operation.

Therefore, for the coil of the system, the biggest impact fault is the open circuit fault of the receiving end. After the fault occurs, the current of the receiving coil drops to zero and the current oscillation of the transmitting coil surges. The current variation during the damage period is related to the electrification parameters of the system. After about $3/\alpha_1$ oscillation, the fault system enters into the steady state.

The steady current variation amplitude of the transmitting end before and after the fault is related to the primary resistance R_1 and L_1/C_1.

When the receiving end of the system is under open circuit fault, a large current impact will occur in the coil. In order to ensure the stable operation of the system, it is necessary to consider the local EMF distribution law of the magnetic shield structure when the receiving end is under open circuit fault condition.

B. CALCULATION METHOD OF EMF

In order to provide wire inlay support and magnetic flux channel to ensure the coupling effect between the two coils, the magnetic shielding structure of the WPT system is usually a multi strand groove structure. The coupling mechanism of the multi strand groove type WPT system described in this paper is composed of a magnetic conducting shielding layer constructed of soft magnetic materials and a multi strand coil as shown in Figure 3(b). The EMF it receives is shown in Figure 3(a). These forces can be divided into the following two types:

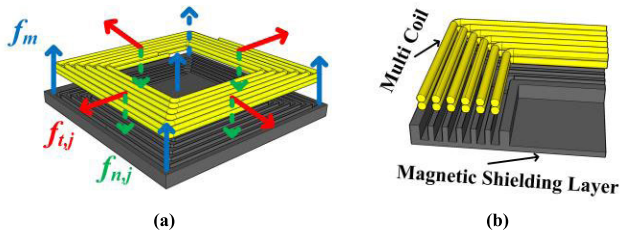

FIGURE 3. The coupling mechanism of the multi groove WPT system: (a) Schematic diagram of EMF on coupling mechanism, (b) Schematic diagram of the composition of coupling mechanism.

1) Electromagnetic forces $f_{t,m}$ and $f_{n,m}$ on the groove wall of the magnetic shielding layer.
2) Electromagnetic forces $f_{t,j}$ and $f_{n,j}$ on the coil.

In reference [20], Calculate the EMF density of magnetic shielding layer by the magnetizing current method:

$$\boldsymbol{f}_m = \boldsymbol{J}_m \times \boldsymbol{B}_m \tag{4}$$

In the formula, $\boldsymbol{J}_m$ is the surface magnetization current density caused by the magnetization effect, $\boldsymbol{B}_m$ is the magnetic induction strength near the magnetic shielding layer, $\boldsymbol{H}_m$ is the magnetic field strength near the magnetic shielding layer, $\boldsymbol{M}$ is the magnetization vector, and vectors $\boldsymbol{n}$ and $\boldsymbol{t}$ are the unit normal vector and unit tangential vector of the closed surface. And satisfy the constitutive equation:

$$\begin{cases} \boldsymbol{B}_m = \mu_0 \boldsymbol{M} + \mu_0 \boldsymbol{H}_m \\ \boldsymbol{J}_m = \nabla \times \boldsymbol{M} \\ \nabla \cdot \boldsymbol{B}_m = 0 \end{cases} \tag{5}$$

Substitute equation (5) into equation (4)

$$\begin{aligned} \boldsymbol{f}_m &= \boldsymbol{J}_m \times \boldsymbol{B}_m \\ &= \nabla \times \boldsymbol{M} \times \boldsymbol{B}_m \\ &= \nabla (\boldsymbol{M} \cdot \boldsymbol{B}_m) - (\nabla \cdot \boldsymbol{M}) \boldsymbol{B}_m \\ &= (\boldsymbol{B}_m \cdot \boldsymbol{M}) \boldsymbol{n} - (\boldsymbol{n} \cdot \boldsymbol{M}) \boldsymbol{B}_m \end{aligned} \tag{6}$$

Under two-dimensional field conditions

$$\begin{aligned} \boldsymbol{B}_m &= \nabla \times \boldsymbol{A}_m = \frac{\delta \boldsymbol{A}_m}{\delta y} \boldsymbol{i} + \frac{\delta \boldsymbol{A}_m}{\delta x} \boldsymbol{j} \\ &= B_{n,m} \boldsymbol{i} + B_{t,m} \boldsymbol{j} \end{aligned} \tag{7}$$

In the formula, $\boldsymbol{A}_m$ is the magnetic vector potential near the magnetic shielding layer, $B_{n,m}$ and $B_{t,m}$ are the normal component and tangential component of magnetic induction strength respectively.

Substitute equation (7) into equation (6), the EMF density of the magnetic shielding structure are obtained as follows:

$$\begin{cases} f_{t,m} = \dfrac{B_{t,m}^2 - B_{n,m}^2}{2\mu_0} \\ f_{n,m} = \dfrac{B_{n,m} \cdot B_{t,m}}{2\mu_0} \end{cases} \tag{8}$$

In the formula, $f_{t,m}$ and $f_{n,m}$ are the tangential component and normal component of EMF density of magnetic shielding layer.

Calculate the EMF density of the coupling coil by Lorentz force law:

$$\boldsymbol{f}_j = S_j J \boldsymbol{L} \times \boldsymbol{B}_j \tag{9}$$

In the formula, J is the current density of the coupling coil, $\boldsymbol{B}_j$ is the magnetic induction strength near the coupling coil, S_j is the cross-sectional area of the coupling coil, and $\boldsymbol{L}$ is the line element.

Under two-dimensional field conditions

$$\begin{aligned} \boldsymbol{B}_j &= \nabla \times \boldsymbol{A}_j = \frac{\delta \boldsymbol{A}_j}{\delta y} \boldsymbol{i} + \frac{\delta \boldsymbol{A}_j}{\delta x} \boldsymbol{j} \\ &= B_{n,j} \boldsymbol{i} + B_{t,j} \boldsymbol{j} \end{aligned} \tag{10}$$

In the formula, $\boldsymbol{A}_m$ is the magnetic vector potential near the coupling coil, $B_{n,j}$ and $B_{t,j}$ are the normal component and tangential component of magnetic induction strength respectively.

Substitute equation (10) into equation (9), the EMF density on the coil unit is:

$$\begin{cases} f_{t,j} = B_{n,j} S_j J L \\ f_{n,j} = B_{t,j} S_j J L \end{cases} \tag{11}$$

In the formula, $f_{t,j}$ and $f_{n,j}$ are the tangential component and normal component of EMF density of the coupling coil.

It is assumed that the coupling mechanism of WPT system is completely elastic and obeys Hooke's law [21]. When the coupling mechanism is subjected to an external force, the deformation of the coupling mechanism will disappear completely if the external force is cancelled. The two-dimensional mechanical vibration of the coupling mechanism of wireless charging system is calculated. The stress-strain relationship at any point is

$$\sigma = \begin{Bmatrix} \sigma_x \\ \sigma_y \\ \tau_{xy} \end{Bmatrix} = \boldsymbol{D}\varepsilon$$

$$= \frac{\boldsymbol{E}}{(1+\alpha)(1-2\alpha)} \begin{bmatrix} 1-\alpha & \alpha & 0 \\ \alpha & 1-\alpha & 0 \\ 0 & 0 & \frac{1-2\alpha}{2} \end{bmatrix} \begin{bmatrix} \varepsilon_x \\ \varepsilon_y \\ \gamma_{xy} \end{bmatrix} \tag{12}$$

In the formula, σ_x, σ_y is the normal stress and τ_{xy} is the shear stress. Corresponding to stress, ε_x, ε_y is normal strain, γ_{xy} is shear strain. $\boldsymbol{D}$ is the elastic matrix, $\boldsymbol{E}$ and α are the elastic model and Poisson's ratio of the elastomer material respectively.

III. SIMULATION ANALYSIS

Front section discusses the changes of the electrical parameters of the WPT system under various fault conditions, and determines that the open load fault has the greatest impact on the WPT system. Selecting the WPT system with groove-shaped magnetic shield structure as the research object. At the same time, combines the field-path coupling time-step finite element method and the Maxwell stress method to establish a mathematical model for calculating the EMF of the WPT system. To discuss the local EMF distribution of the grooved magnetic shielding structure when the load is open, Field-circuit coupled time step model of the multi groove WPT system is built through the finite element analysis software, which is shown in Figure 4. As shown in Table. 2, the parameters of the coupling mechanism of the simulation model are shown.

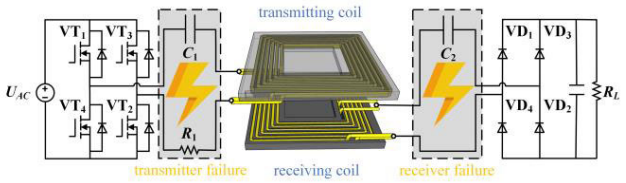

FIGURE 4. Field-path coupled time step model for WPT system.

TABLE 2. Field-path coupling time step model coupling mechanism parameters.

Parameter name	Setting value	Description
f	10 kHz	Resonant frequency
r	4 mm	Line diameter
n	6	Number of coil turns
R	22.6 cm	Coil semi-diameter
d	2 cm	Turn pitch
h	12 cm	Transmission distance
P	3 kW	Transmitting power

Figure 5 shows the chart of magnetic induction strength distribution of WPT system. In the stable state, the magnetic induction strength distribution of WPT system is as shown in Figure 5(a). There is a strong distribution of magnetic induction strength at the back plate of magnetic conduction shielding layer, and the maximum value of magnetic induction strength is 116.5mT. At the same time, there is a strong

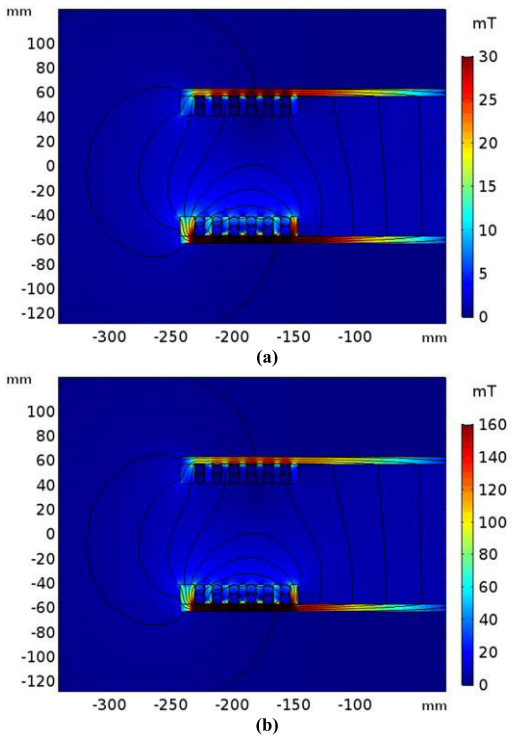

FIGURE 5. Magnetic induction strength distribution of WPT system: (a) In normal state, (b) After open circuit fault at receiving end.

magnetic induction strength force on the side wall of the edge groove due to multiple coils; the distribution of the magnetic induction strength after the open circuit fault at the receiving end reaches a stable state, which is shown in Figure 5(b). The distribution of the magnetic induction strength before and after the fault is similar, and the maximum value of the magnetic induction strength is 514.2mT.

The surface stress distribution is positively correlated with the coil current at the end, so the surface stress amplitude of the coupling mechanism at the transmitting end is higher than that of the coupling mechanism at the receiving end. This paper only discusses the surface stress distribution of the coupling mechanism at the transmitting end. As shown in Figure 6, the surface stress distribution of the coupling mechanism at the transmitting end of the WPT system is shown. The surface stress distribution of the coupling mechanism at the transmitting end of the WPT system in the stable state, which is shown in Figure 6(a). The surface stress of the system is jointly contributed by Maxwell force and Lorentz force. In the multi strand groove structure, there is a strong stress distribution on the side wall surface of the edge groove and the tip of each groove. At the same time, the contact between the strand forming coil and the groove side wall and the contact between the strand forming coils in the same groove produce extrusion, as shown in Figure 6(b). The surface stress distribution of the coupling mechanism at the transmitting end is similar before and after the fault. The amplitude ratio of the surface stress of the coupling

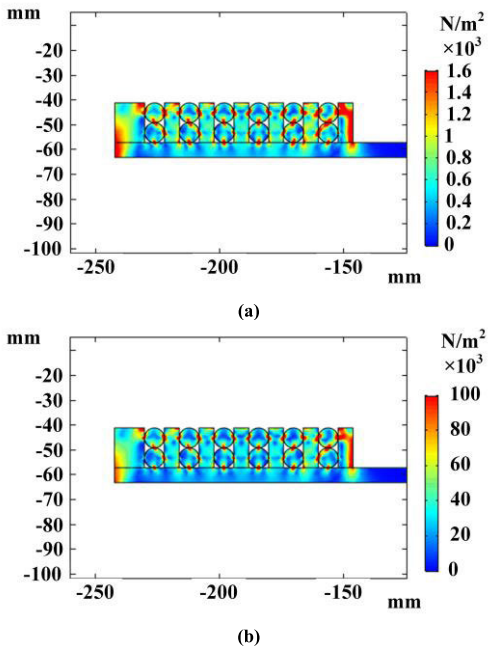

FIGURE 6. Surface stress distribution diagram of the coupling mechanism at the transmitting end: (a) In normal state, (b) After open circuit fault at receiving end.

mechanism before and after the sudden open circuit fault at the receiving end of the WPT system is 1:16 square of the fault current ratio.

Figure 7 shows the stress of the magnetic shielding layer at the transmitting end and the magnetic shielding layer at the receiving end after the open circuit fault at the receiving end. The amplitude of the EMF on the magnetic shielding layer at the transmitting end is about 2.9N under the steady-state operation. The increase of the coil current oscillation at the transmitting end after the fault causes the EMF on the magnetic shielding layer at the transmitting end to rise until it is stable, and its steady-state amplitude is about 19 times of that under the normal state; The amplitude of the EMF on the magnetic shielding layer at the receiving end is about 0.8N under steady-state operation. The increase of the coil current oscillation at the transmitting end after the fault causes the increase of the amplitude of the high-frequency

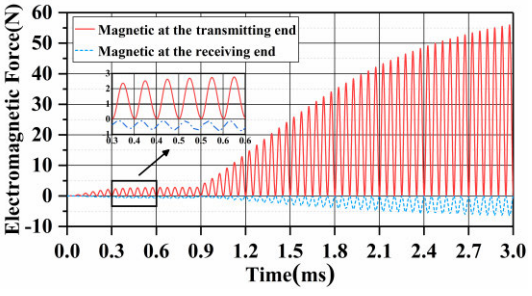

FIGURE 7. Force of the transmitting end magnet and the receiving end magnet.

magnetic induction strength. Therefore, the EMF on the magnetic shielding layer at the receiving end reaches to a stable state, and its steady-state amplitude is about 6 times of the steady-state amplitude under normal state.

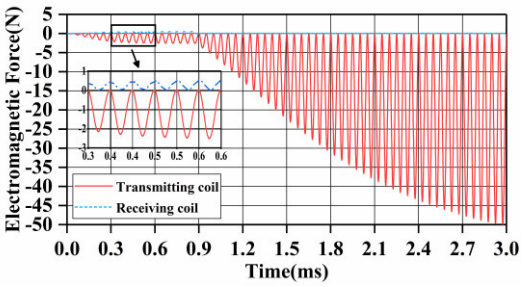

FIGURE 8. Force of the transmitting end coil and the receiving end coil.

Figure 8 shows the stress of the coil at the transmitting end and the coil at the receiving end after the open circuit fault at the receiving end. The amplitude of the EMF on the coil at the transmitting end under steady-state operation is about 2.5N. After the fault occurs, the EMF oscillation on the coil at the transmitting end tends to a stable state, and its steady-state amplitude is about 20 times of that under normal state. The amplitude of the EMF on the coil at the receiving end under steady-state operation is about 0.5N, and the current of the coil at the receiving end drops to zero after the fault occurs, so the EMF of the coil at the receiving end after the fault is zero.

Through the simulation of the stress of the coupling structure before and after the open circuit fault of the receiving end of the multi channel WPT system, it can be seen that the surface stress of the system is jointly contributed by Maxwell force and Lorentz force, and the distribution of the surface stress before and after the fault is similar. The EMF distribution of the coupling mechanism is consistent with that of the spatial magnetic induction strength. Due to the particularity of the multi strand groove structure, the magnetic induction strength distribution on the groove wall of the magnetic shielding layer is strong, resulting in a strong surface stress on the inner groove wall. At the same time, the magnetic induction strength at the tip of the groove is higher than that in the adjacent area, resulting in a strong stress distribution. Under the action of Lorentz force in the alternating magnetic induction strength, the coil shows contraction and expansion movement in the horizontal direction, which produces extrusion on the groove wall; in the vertical direction, it presents vibration phenomenon, collides with the coil in the groove, and produces extrusion on the groove wall at the bottom of the groove. The surface stress amplitude ratio of coupling mechanism before and after fault is about the square of fault current ratio.

After the open circuit fault occurs in the receiving end of the multi channel WPT system, the spatial magnetic induction strength increases due to the surge of the coil current oscillation at the transmitting end. The EMF on the electromagnetic

shielding layer of the transmitting end and the receiving end will oscillate and increase with it. After about 40 oscillation periods, the EMF will tend to be stable, and the vibration period of the EMF is twice of the resonant vibration frequency of the system. Before and after the fault, the steady-state amplitude increase rate of the EMF applied on the magnetic shielding layer of the transmitting end is about the square of the current increase rate. After the open circuit fault occurs in the receiving end of the multi channel WPT system, the change rule of the EMF on the transmitting coil is the same as that on the magnetic shielding layer, which is stable after about 2 times of the fault vibration current cycle. The current in the receiving coil will be zero due to the open circuit fault of the receiving end, so the EMF received will be reduced to zero.

IV. EXPERIMENTAL RESULTS

In order to verify the distribution of EMF under the worst fault condition of the above-mentioned multi channel WPT system, a test platform for the WPT system with the electrical parameter index and the structural parameter index consistent with the field-circuit coupled time step model parameter setting is built as shown in Figure 9(a), and the open circuit fault of the receiving end is simulated. The high frequency dynamic force sensor is used to measure the test point of coupling mechanism of the transmitting end as shown in Figure 9(c) and the stress of the coupling mechanism of the multi groove WPT system is analyzed. Figure 9(b) shows a mechanical probe signal acquisition device.

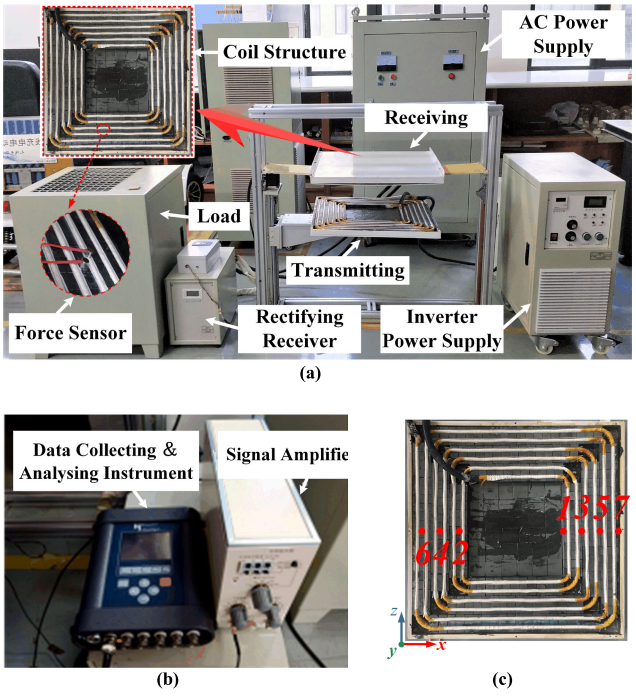

FIGURE 9. WPT system test platform. (a) WPT system, (b) Mechanical probe signal acquisition device, (c) Test point.

The surface stress of the coupling mechanism under the worst fault condition is simulated by the test platform of the WPT system. The figure shows the forces on the coupling mechanism of the transmitting end at different test points. It can be seen from Figure 10 that at a certain time after the open circuit fault occurs at the receiving end of the system, the EMF on the surface of the coupling mechanism at the transmitting end surges sharply. After about 2ms, the force on the coupling mechanism tends to be stable. The phases of the EMF at different test points at the same time are the same. The EMF distribution on the surface of the coupling mechanism has the rule of high in the middle and low in both sides. The simulation results are consistent with those of the WPT system under the fault condition at the same test point.

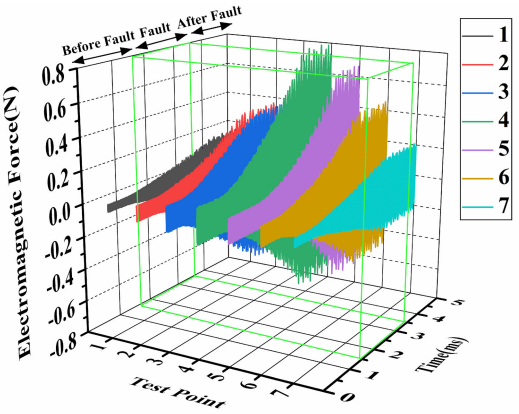

FIGURE 10. EMF at different test points.

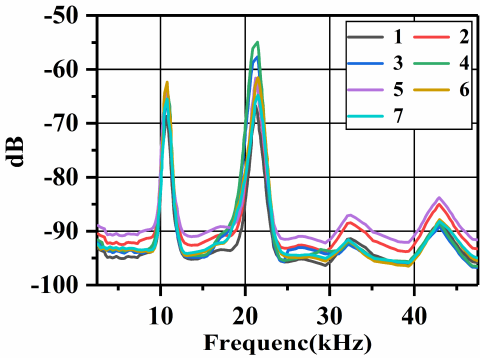

FIGURE 11. Spectrogram of EMF at different test points.

Figure 11 shows the spectrum diagram of EMF after open circuit fault of load end of multi strand groove type WPT system at different test points. The main frequency of EMF of coupling mechanism is 21.78kHz, which is twice of the resonant frequency of the system. The EMF of the coupling mechanism mainly includes the fundamental and even frequency components, which is consistent with the simulation results.

As shown in Figure 12, the RMS comparison of the EMF before and after the open circuit fault of the load end of the

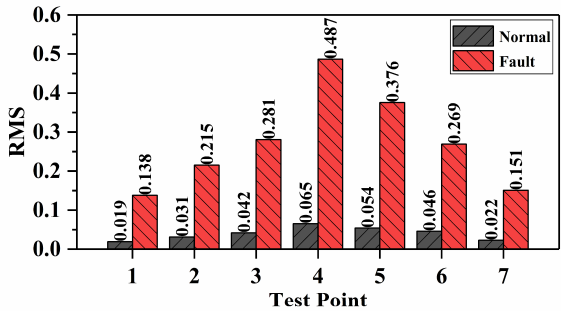

FIGURE 12. RMS value of EMF at different test points before and after failure.

multi channel WPT system at different test points is made. Before the open circuit fault at the receiving end occurs, test point 4 is the place of the maximum force with the value of 0.065N. As the test point moves to both sides, the EMF on the part near the outside decreases. Due to the asymmetry of the structure of the magnetic shielding layer, the descending rate of the moving direction near the outside of the coupling mechanism is smaller than that near the inside of the coupling mechanism. After the open circuit fault at the receiving end occurs, the EMF at each test point increases significantly, and the increase rate of the EMF at the same test point before and after the fault is about 7 times. Among them, test point 4 is the place of the maximum force with the value of 0.487N. The distribution of EMF at different test points is consistent with that before fault occurs.

In order to verify the EMF distribution of the coupling mechanism after the open circuit fault of the front section to the multi strand groove type WPT system, the open circuit fault simulation test platform of the WPT system is built, and the surface stress of the coupling mechanism of the WPT system is measured by high frequency force probe. According to the analysis of the experimental data, the amplitude of the EMF on the coupling mechanism is proportional to the square of the coil current. The distribution of the EMF on one side of the coupling mechanism is high in the middle and low on both ends. At the same time, the descent rate near the outside of the coupling mechanism is lower than that near the inside of the coupling mechanism. This phenomenon is consistent with the surface stress distribution of the coupling mechanism at the transmitting end of the front section of the multi strand groove type WPT system. The Maxwell force on the magnetic shielding layer of the coupling mechanism is closely related to the magnetic induction strength distribution. The asymmetry of the spatial magnetic induction strength distribution results in the asymmetry of the surface stress distribution.

V. SMOOTHING SCHEME

A. VARIABLE-TURN-PITCH PLANAR COIL

By analyzing the characteristics of EMF, the distribution of EMF is related to the distribution of magnetic induction strength. At the same time, the magnetic induction strength distribution is related to the material properties, winding mode, shape structure and relative position of the coil. To constrain the magnetic induction strength, a variable-turn-pitch planar coil structure is proposed. By optimizing the design of the turn pitch of the coil, the constrained control of the magnetic induction strength is realized, and the EMF on the coupling mechanism is weakened. Figure 13 shows the variable-turn-pitch planar coil proposed in this paper.

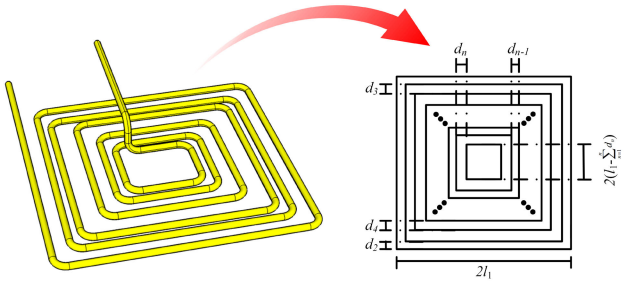

FIGURE 13. Variable-pitch planar coil diagram.

To simplify the analysis, the coil can be equivalent to a group of concentric square coils nested with each other, and the distance between adjacent square coils is a non-fixed constant. Name the coils in turn from the outside to the inside, and define the distance between the $(n-1)$-th turn and the n-th turn of the square coil as d_n, and specify $d_1 = 0$, then the side length of the i-th square coil meets:

$$2l_i = 2l_1 - \sum_{n=1}^{i} 2d_n \tag{13}$$

In the formula, $2l_1$ is the side length of the outermost square coil.

According to Biot-Savart law, the magnetic induction strength of the i-turn square coil at any point $P\ (x, y, z)$ in space is obtained as follows:

$$B_i = \frac{\mu I}{4\pi}\chi_i\ (l_i, x, y, z) \tag{14}$$

In the formula, I is the coil current, l_i is the side length of the i-th turn square coil.

According to the superposition theorem, the magnetic induction strength intensity of the variable-turn-pitch planar coil at any point $P\ (x, y, z)$ in space is obtained as follows:

$$\begin{aligned} B &= \frac{\mu I}{4\pi}\chi\ (x, y, z, l_1, l_2, l_3 \cdots l_n) \\ &= \frac{\mu I}{4\pi}\delta\ (x, y, z, d_1, d_2, d_3 \cdots d_n) \end{aligned} \tag{15}$$

According to the inductance formula of the coil, the inductance of the variable-turn-pitch planar coil is obtained as follows:

$$\begin{aligned} L &= \frac{\Phi}{I} = \sum \frac{B_i l_i^2}{I} \\ &= \sum \frac{\mu l_i^2}{4\pi}\chi_i\ (l_i, x, y, z) \\ &= \frac{\mu}{4\pi}\gamma\ (d_1, d_2, d_3 \cdots d_n) \end{aligned} \tag{16}$$

The mutual inductance between the i-th turn square coil on one side and the j-th turn square coil on the other side can be expressed as:

$$M_{ij} = \frac{\Phi_{ij}}{I} = \frac{2\mu_0}{\pi}\alpha_{ij}\left(z, l_i, l_j\right) \tag{17}$$

In the formula, z is the vertical distance between the coils

According to the superposition law, the mutual inductance between the transmitting coil and the receiving coil is obtained as follows:

$$\begin{aligned} M &= \sum_{i=1}^{N}\sum_{j=1}^{N} M_{ij} = \alpha\left(z, l_1, l_2, l_3 \cdots l_n\right) \\ &= \beta\left(z, d_1, d_2, d_3 \cdots d_n\right) \end{aligned} \tag{18}$$

When the turn pitch variable of variable-turn-pitch planar coil changes, on the one hand, the magnetic induction strength in the coupling space changes, on the other hand, the coil electrical parameters also changes.

B. EMF SMOOTHING MODEL

From the previous analysis, it can be known that optimizing the turn pitch of the variable-turn-pitch planar coil can realize the constrained control of the spatial electromagnetic field, and further weaken the EMF of the coupling mechanism. Aiming at the problem of the EMF of the coupling mechanism under failure, the equi-turn plane coil with multi strand groove structure is used as the initial optimization object to smooth the EMF of the coupling mechanism under failure.

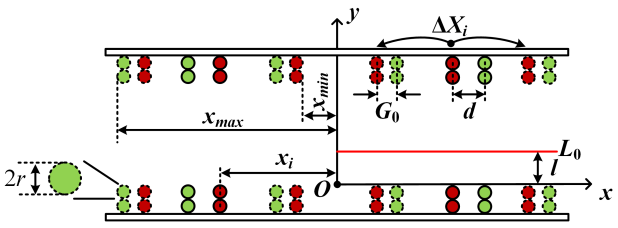

FIGURE 14. Schematic diagram of optimization model.

Figure 14 is schematic diagram of smoothing model. The tangent line L_0 parallel to the plane coil is used as the optimization area. The movable position of the i-th coil is ΔX_i, and the wire diameter of each coil is r. At the same time, considering the coil processing size limit and the use site limit, specify the minimum inner diameter and maximum outer diameter of the target coil as $x_{\min}$ and $x_{\max}$, respectively.

TABLE 3. Optimization model indicators.

Parameter name	Setting value	Description
x_{min}	0.3 cm	Minimum inner diameter
x_{max}	22.6 cm	Maximum outer diameter
G_0	0.4 cm	Minimum interval
l	0 cm	Optimize regional location
η_{min}	90%	Minimum transmission efficiency

TABLE 4. Optimization results.

Position	Before optimization/cm	After optimization/cm
x_1	12.20	0.74
x_2	14.20	2.19
x_3	16.20	6.00
x_4	18.20	15.16
x_5	20.20	20.14
x_6	22.20	22.20

To ensure the sequence between each turn of the coil after optimization, the minimum interval between adjacent coils is specified as G_0, and $\eta_{\min}$ is specified as the minimum transmission efficiency aims.The optimization goals and constraints can be expressed as (19), shown at the bottom of the page.

Table. 3 shows the optimization model indicators. The tangent line at 0cm from the surface of the transmitting coil is selected as the optimization area.

C. THE SUM OF MAGNETIC INDUCTION STRENGTH

The SNOPT algorithm is used to optimize the turn pitch of the variable-turn-pitch planar coil. Before optimization, the coupling coil is equi-turn-pitch distribution. After optimization, the turn pitch of the coupling coil is re-arranged. As shown in Table. 4, the coil position of each turn is optimized. Figure 15 shows the distribution of magnetic induction strength of the optimized system under the open circuit fault at the receiving end, the sum of the magnetic induction strength is significantly improved compared to before optimization.

Figure 16 shows the distribution of the magnetic induction strength on L_0 under the open circuit fault at the receiving

$$\begin{aligned} &\underset{d_1,d_2,d_3,\cdots,d_n}{\text{minimize:}} \ \frac{1}{L_0}\int_{L_0} Bdl \\ &\text{subject to: } (2i-1)r - x_i - x_{\min} \le \Delta X_i \le x_{\max} - x_i - [2(n-i)+1]r \quad (i = 1, 2, 3, \cdots, n) \\ &\qquad G_0 \le (d + \Delta X_{i+1} - \Delta X_i) \quad (i = 1, 2, 3, \cdots, n-1) \\ &\qquad \eta \ge \eta_{\min} \end{aligned} \tag{19}$$

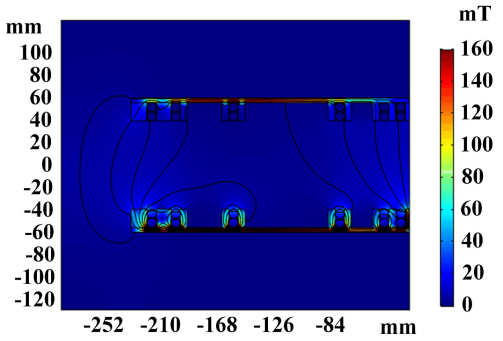

FIGURE 15. Magnetic induction strength distribution after optimization.

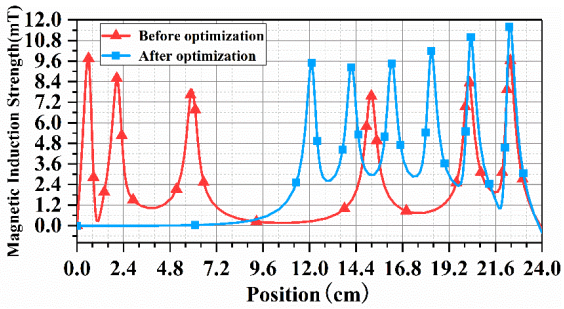

FIGURE 16. Magnetic induction strength distribution on tangent line.

end before and after optimization. The maximum magnetic induction strength on the tangent line before optimization is 11.72mT, and the maximum magnetic induction strength after optimization is 9.83mT. After optimization, the maximum magnetic induction strength decreased by 16.16%. The average values of the magnetic induction strength on the tangent line before and after optimization were 5.84mT and 4.71mT, respectively. After optimization, the average value of the magnetic induction strength decreased by 19.32%.

D. EMF OF COUPLING MECHANISM

Figure 17 shows the comparison of EMF on the coupling mechanism of transmitting end under the open circuit fault at the receiving end before and after optimization. After optimization, the EMF on the coil of transmitting end decreased by 21.83%. The EMF on the magnetic shielding layer of transmitting end decreased by 27.41%. For the EMF of the entire structure of the coupling mechanism, the EMF of

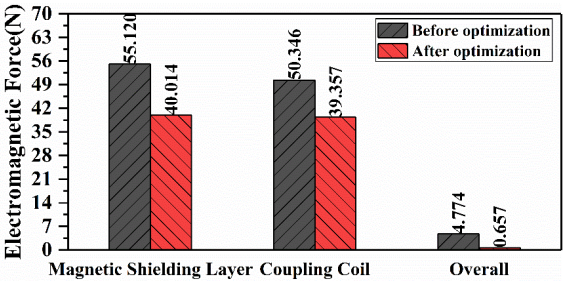

FIGURE 17. Comparison chart of EMF of coupling mechanism.

the coupling mechanism on the transmitting end is reduced by 86.24%.

By optimizing the structure of the variable-turn-pitch planar coil, the EMF of the coupling mechanism under the open circuit fault at the receiving end is significantly weakened. Combined with the performance of the sum of magnetic induction strength in the coupling space of the system under the open circuit fault at the receiving end before and after optimization, the feasibility of the EMF smoothing scheme based on the variable-turn-pitch planar coil is verified.

VI. CONCLUSION

In this paper, the local EMF distribution of the coupling mechanism under the worst fault condition of the multi groove WPT system is studied, and propose an effective smoothing scheme. The main results are as follows.

- the change of coil current under the typical fault of WPT system based on the SS type is analyzed, and the worst fault condition for the coil of the system is determined to be the sudden open circuit at the receiving end, when the coil at the transmitting end will produce a large current impact. The time constant of the dynamic circuit is related to the attenuation coefficient α_1 of the transmitting end, and the amplitude change of the steady-state current of the transmitting end before and after the fault is related to the primary resistance R_1 and L_1/C_1.
- The field-circuit coupled time step model of multi channel WPT system is built to obtain the spatial magnetic induction strength distribution and the surface stress distribution of the coupling mechanism before and after the fault. The distribution of the two is consistent. The inner groove wall and the tip of each groove have strong magnetic induction strength distribution, and the surface stress is strong. At the same time, in the horizontal direction, the multi coil continues to contract and expand in the high-frequency alternating magnetic induction strength, showing zero. In the vertical direction, the multi coil vibrates, collides with the groove coil, and compresses the groove wall at the bottom of the groove.
- Use the WPT system test platform to simulate the open circuit fault of the burst receiving end. The coupling mechanism is divided into test areas and the force information of the coupling mechanism surface is collected through the high frequency force probe. The distribution law of EMF on the surface of coupling mechanism is high in the middle and low in both ends. The vibration period of EMF is twice of the resonant vibration frequency of the system, and the increase rate of EMF on the same test point before and after the fault is about 7 times.
- Through the SNOPT algorithm, the optimal solution of each turn pitch variable is obtained, and the degree of restraint of the magnetic induction strength after optimization is increased by 19.32%. For the EMF of the entire structure of the coupling mechanism under the

open circuit fault at the receiving end, the EMF of the coupling mechanism on the transmitting end is reduced by 86.24%.

REFERENCES

[1] S. Y. R. Hui, W. Zhong, and C. K. Lee, "A critical review of recent progress in mid-range wireless power transfer," *IEEE Trans. Power Electron.*, vol. 29, no. 9, pp. 4500–4511, Sep. 2014, doi: 10.1109/TPEL.2013.2249670.

[2] S. Li and C. C. Mi, "Wireless power transfer for electric vehicle applications," *IEEE J. Emerg. Sel. Topics Power Electron.*, vol. 3, no. 1, pp. 4–17, Mar. 2015, doi: 10.1109/JESTPE.2014.2319453.

[3] A. P. Sample, D. A. Meyer, and J. R. Smith, "Analysis, experimental results, and range adaptation of magnetically coupled resonators for wireless power transfer," *IEEE Trans. Ind. Electron.*, vol. 58, no. 2, pp. 544–554, Feb. 2011, doi: 10.1109/TIE.2010.2046002.

[4] R. Zhang and C. K. Ho, "MIMO broadcasting for simultaneous wireless information and power transfer," *IEEE Trans. Wireless Commun.*, vol. 12, no. 5, pp. 1989–2001, May 2013, doi: 10.1109/TWC.2013.031813.120224.

[5] M. Rozman, A. Ikpehai, B. Adebisi, K. M. Rabie, H. Gacanin, H. Ji, and M. Fernando, "Smart wireless power transmission system for autonomous EV charging," *IEEE Access*, vol. 7, pp. 112240–112248, 2019, doi: 10.1109/ACCESS.2019.2912931.

[6] K. Fotopoulou and B. W. Flynn, "Wireless power transfer in loosely coupled links: Coil misalignment model," *IEEE Trans. Magn.*, vol. 47, no. 2, pp. 416–430, Feb. 2011, doi: 10.1109/TMAG.2010.2093534.

[7] H.-M. Ahn, Y.-H. Oh, J.-K. Kim, J.-S. Song, and S.-C. Hahn, "Experimental verification and finite element analysis of short-circuit electromagnetic force for dry-type transformer," *IEEE Trans. Magn.*, vol. 48, no. 2, pp. 819–822, Feb. 2012, doi: 10.1109/TMAG.2011.2174212.

[8] F. Lin, S. Zuo, W. Deng, and S. Wu, "Modeling and analysis of electromagnetic force, vibration, and noise in permanent-magnet synchronous motor considering current harmonics," *IEEE Trans. Ind. Electron.*, vol. 63, no. 12, pp. 7455–7466, Dec. 2016, doi: 10.1109/TIE.2016.2593683.

[9] J. D. Mina-Casaran, D. F. Navas, and D. F. Echeverry-Ibarra, "Evaluation of the audible noise level on distribution transformers using the Sound Pressure Method," *Revista Facultad de Ingeniería*, vol. 26, no. 45, pp. 71–82, 2017, doi: 10.19053/01211129.v26.n45.2017.6051.

[10] P. Shuai and J. Biela, "Influence of material properties and geometric shape of magnetic cores on acoustic noise emission of medium-frequency transformers," *IEEE Trans. Power Electron.*, vol. 32, no. 10, pp. 7916–7931, Oct. 2017, doi: 10.1109/TPEL.2016.2636572.

[11] Y. Li, Q. Lu, and Z.-Q. Zhu, "Unbalanced magnetic force prediction in permanent magnet machines with rotor eccentricity by improved superposition method," *IET Electr. Power Appl.*, vol. 11, no. 6, pp. 1095–1104, Jul. 2017, doi: 10.1049/iet-epa.2016.0739.

[12] X. Wang, X. Wang, M. Li, and M. Lu, "Reconfigurable wireless power transmission in fully-enclosed space using antenna array," *IEEE Access*, vol. 7, pp. 173098–173110, 2019, doi: 10.1109/ACCESS.2019.2956889.

[13] X. Zhang, Q. Yang, Y. Cui, H. Liu, and L. Jin, "Design, optimization and verification of energy transmit coils for high power wireless energy transmission systems," *Trans. China Electrotech. Soc.*, vol. 28, no. 10, pp. 12–18, 2013.

[14] B. Wei, S. Wang, X. Wu, H. Meng, and X. Zhang, "Research on synergetic working mode of magnetic resonance based on γ Matching," *Trans. China Electrotech. Soc.*, vol. 33, no. S2, pp. 278–286, 2018.

[15] X. Zhang, X. Ni, B. Wei, S. Wang, and Q. Yang, "Characteristic analysis of electromagnetic force in a high-power wireless power transfer system," *Energies*, vol. 11, no. 11, p. 3088, Nov. 2018, doi: 10.3390/en11113088.

[16] X. Zhang, Z. Yuan, Q. Yang, H. Meng, Y. Jin, Z. Wang, and S. Jiang, "High-frequency electromagnetic force characteristics on electromagnetic shielding materials in wireless power transmission system," in *Proc. IEEE PELS Workshop Emerg. Technol., Wireless Power Transf. (WoW)*, May 2017, pp. 1–5.

[17] D. Kim, M. Kim, J. Yoo, H.-H. Park, and S. Ahn, "Magnetic resonant wireless power transfer for propulsion of implantable micro-robot," *J. Appl. Phys.*, vol. 117, no. 17, 2015, Art. no. 17E712.

[18] D. Kim, J. Park, K. Kim, H.H. Park and S. Ahn, "Propulsion and control of implantable micro-robot based on wireless power transfer," in *Proc. IEEE Wireless Power Transf. Conf. (WPTC)*, May 2015, pp. 1–4.

[19] Z. ZhaoF Liu and K. Chen, "Summary of research on wireless charging technology for electric vehicles," *Trans. China Electrotech. Soc.*, vol. 31, no. 20, pp. 30–40, 2016.

[20] C. Chen, X. Huang, W. Sun, L. Tan, and H. Qiang, "Influence of metal obstacles on magnetically coupled resonant wireless energy transmission system," *Trans. China Electrotech. Soc.*, vol. 29, no. 9, pp. 22–26, 2014.

[21] M. Besbes, Z. Ren, and A. Razek, "Finite element analysis of magneto-mechanical coupled phenomena in magnetostrictive materials," *IEEE Trans. Magn.*, vol. 32, no. 3, pp. 1058–1061, May 1996, doi: 10.1109/20.497423.

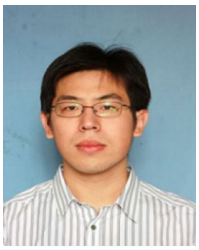

XIAN ZHANG received the M.E. and Ph.D. degrees in electrical engineering from the Hebei University of Technology, Tianjin, China, in 2009, and 2012, respectively. He is currently a Professor with the School of Electrical Engineering and Automation, Tiangong University, Tianjin. His current research interest includes wireless power transfer and its application.

FENGXIAN WANG was born in Henan, China, in 1995. He received the B.S. degree in electrical engineering and automation from the School of Electrical Engineering and Automation, Tiangong University, Tianjin, China, in 2020. His current research interest includes wireless power transfer and its applications.

XUEJING NI was born in Heilongjiang, China, in 1996. She received the M.E. degree in electrical engineering and automation from Tiangong University, Tianjin, China, in 2017, where she is currently pursuing the M.E. degree in electrical engineering. Her current research interest includes wireless power transfer and its applications.

YANAN REN was born in Ningxia, China, in 1997. She received the B.S. degree in automation from the Hebei University of Engineering, in 2019, where she is currently pursuing the M.E. degree in electrical engineering. Her current research interest includes wireless power transfer and its applications.

QINGXIN YANG received the B.S., M.S., and Ph.D. degrees from the Hebei University of Technology, Tianjin, China, in 1983, 1986, and 1997, respectively. He is currently the President of Tianjin Polytechnic University, Tianjin, China. His current research interests include electromagnetic field computation and wireless power transfer. He is a Board Member of the International COMPUMAG Society and the President of the China Electrotechnical Society.